High-Power Laser Testing of Phenolic Impregnated Carbon Ablators Under Flight-Relevant Heat-Flux Conditions

Matthew Stewart[1], Natalie Victory[2], and Ryan Finn[3]
The University of Tennessee-Knoxville, Knoxville, TN, 37996, USA

Lula Jane Abbott [4]
Institut National des Sciences Appliquées, Rennes, Bretagne, 35000, France

Zhili Zhang[5]
The University of Tennessee-Knoxville, Knoxville, TN, 37996, USA

Impregnated carbon ablators offer favorable thermal and mechanical characteristics for extreme heat-flux environments, yet their coupled chemical outgassing and internal structural degradation under thermal loading leaves questions about undiscovered weaknesses. This paper presents a combined experimental investigation conducted in two phases to characterize both the volatile emission behavior and microstructural damage of the phenolic-impregnated carbon ablator, DragonPlate™, subjected to high-power laser heating. In the first phase, samples were heated using a continuous-wave high-power diode laser (LDM 500-60, 910 nm, up to 500 W) in a helium atmosphere, reaching surface temperatures of approximately 1350 °C with estimated ablation heat fluxes up to 541 W/cm². Quantitative measurements revealed significant outgassing of phenol (C_6H_5OH) and hydrogen (H_2), directly linking the release of volatiles to the decomposition of phenolic resin. In the second phase, six additional samples were tested under similar laser conditions with an effective applied power density of approximately 470 W/cm² in a reduced-pressure argon environment (~1×10^{-3} Torr), reaching peak surface temperatures of approximately 1085 °C. Post-test characterization using X-ray micro-computed tomography (Zeiss Xradia Context MicroCT) revealed internal structural damage at the bonding and pore scale. Prior and post-test mass measurements showed an average mass loss of 0.265 g from an initial average sample mass of 2.53 g, confirming resin loss through outgassing or liquidation. These results demonstrate that carbon ablators undergo significant physical and material changes under sustained, flight-relevant high-power laser heating. The observed mass loss, internal damage at bonding interfaces, and pore-scale alterations indicate substantial modification of the impregnated carbon system when subjected to extreme heat-flux conditions representative of aerospace thermal protection environments.

[1] Undergraduate Research Asst., Department of Mechanical and Aerospace Engineering, AIAA University Student Member 1923630.
[2] Undergraduate Research Asst., Department of Mechanical and Aerospace Engineering, AIAA University Student Member 1584415.
[3] Undergraduate Research Asst., Department of Mechanical and Aerospace Engineering, AIAA University Student Member 1924076.
[4] Summer Intern, Department of Mechanical and Aerospace Engineering.
[5] Professor, Dept. of Mechanical, Aerospace, and Biomedical Engineering, University of Tennessee, and AIAA Associate Fellow.

I. Nomenclature

PICA = Phenolic Impregnated Carbon Ablator
TPS = Thermal Protection Systems
CT = Computed Tomography
MS = Mass Spectrometer

II. Introduction

Phenolic-Impregnated Carbon Ablators (PICA) are a class of thermal protection system (TPS) materials well known for their lightweight structure, low thermal conductivity, and exceptional resistance to ablation. This makes them ideal choices for atmospheric entry and high-speed aerospace applications. These desirable characteristics have attracted significant interest, particularly following PICA's successful application as the heat shield for NASA's 2020 Perseverance rover mission to Mars [1]. As one of the few material systems capable of withstanding the intense thermal and mechanical stresses encountered during interplanetary atmospheric entry, PICA now serves as a standard in the development of next-generation TPS technologies. Its proven performance under extreme conditions highlights the need for continued experimental research to better understand the degradation and effective life span. Surface heat flux is a primary driver of TPS performance in hypersonic and planetary-entry environments. For blunt-body aeroshells and stagnation regions, convective heat fluxes during Earth and Mars entry typically range from tens to several hundreds of watts per square centimeter, with peak values approaching or exceeding 500 W/cm² for high-velocity trajectories, high ballistic coefficients, and steep entry angles. Localized heating near stagnation points and leading edges can further elevate surface heat flux beyond mission-averaged values [2]. Consequently, imposed heat fluxes on the order of 500 W/cm² represent a critical and flight-relevant regime for evaluating TPS material response, enabling assessment of ablation onset, mass loss, and thermal stability during the most demanding phases of hypersonic flight.

A wide range of experimental methods has been employed to investigate the performance of PICA and related materials, including testing in arc jet facilities and with oxy-acetylene torch configurations [3]. While these methods have provided valuable insight, they often introduce complex flow dynamics or chemical contamination, such as plasma effects or combustion byproducts, that can obscure material-specific responses and data collection. Specifically, these testing platforms often incur high operational costs and limited throughput. As a conscious alternative, high-power continuous-wave diode lasers offer a non-intrusive, repeatable, and precisely controlled means of simulating high-enthalpy surface heating, enabling more isolated observation of ablation behavior and thermal degradation processes. This study investigates DragonPlate™, which is a commercial phenolic-impregnated carbon composite as a testing substitute for traditional PICA materials. Two phases of laser-based experimentation are conducted to characterize both the chemical outgassing behavior and the internal structural damage of the material under simulated flight-relevant thermal loading. In the first phase, samples are exposed to a high-power diode laser (LDM 500-60, 910 nm) in a helium atmosphere, and measurements of the gas composition are taken in a mass spectrometer. The second phase utilizes six additional samples subjected to similar laser heating in a low-pressure argon environment, focused on time-dependent effects by observing the structural degradation resulting from prolonged exposure.

III. Experiments

A. Experimental Setups

The experimental tests were conducted in two distinct phases, each focusing on a separate parameter. In the first phase of experiments, an integrated testbed combining a diode laser, mass spectroscopy, and a helium environment-controlled chamber was used to characterize the thermal and chemical response of the DragonPlate™ specimen under prescribed laser heating, as diagrammed in Figure 1. A Laserline (LDM 500-60) continuous-wave diode laser (λ = 910 nm) provided the imposed surface heat flux with a power rise time of approximately 0.1 ms. The laser output was modulated using a programmable function generator that generated a time-dependent 0-5 V control signal to the laser control module. Laser energy was delivered to the target via optical fibers to maintain beam quality and minimize transmission losses and divergence. At the laser head, a 200 mm focal-length lens produced an 11 mm × 11 mm "top-hat" profile on the sample surface, yielding a maximum theoretical power density of approximately 500 W/cm².

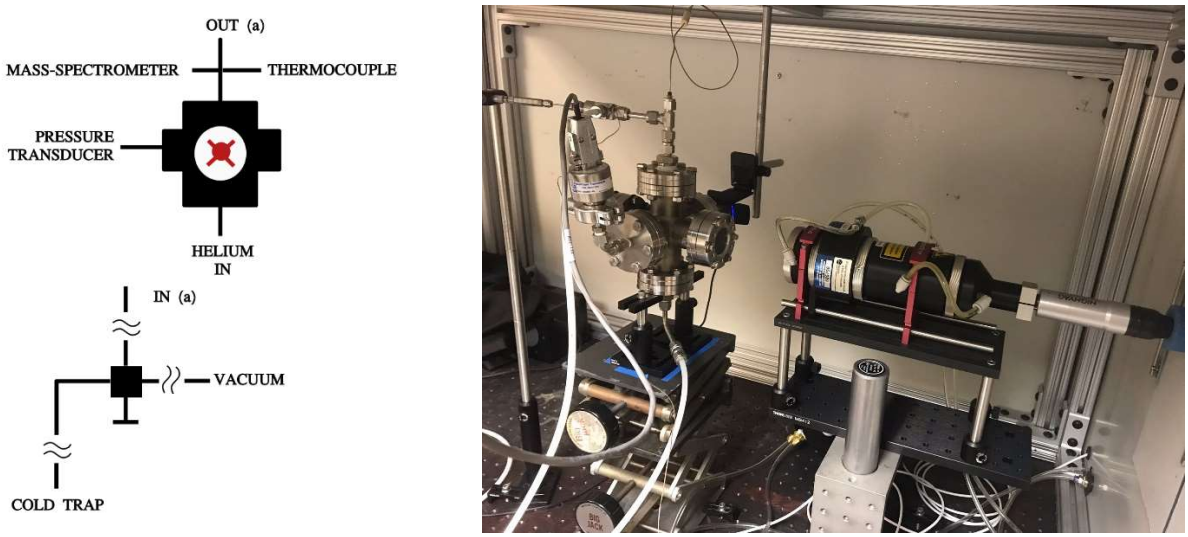

Fig. 1a (left) & 1b (right) Diagram of Phase 1 Experimental Setup Showing the Chamber Inputs and Outputs

Gas composition during laser exposure was monitored in real time using a Hiden Analytical RD-series mass spectrometer integrated with the chamber. The instrument operated under high-vacuum conditions and measured species up to 200 amu with a detection limit in the parts-per-billion (ppb) range, enabling sensitive detection of volatile compounds and reaction products released from the material during heating. The custom steel chamber provided the controlled test environment and was instrumented with a type K thermocouple for temperature measurement and an MKS Piezo Pirani pressure transducer to track pressure evolution. Together, these diagnostics enabled time-resolved characterization of temperature and pressure variations throughout the experimental procedure.

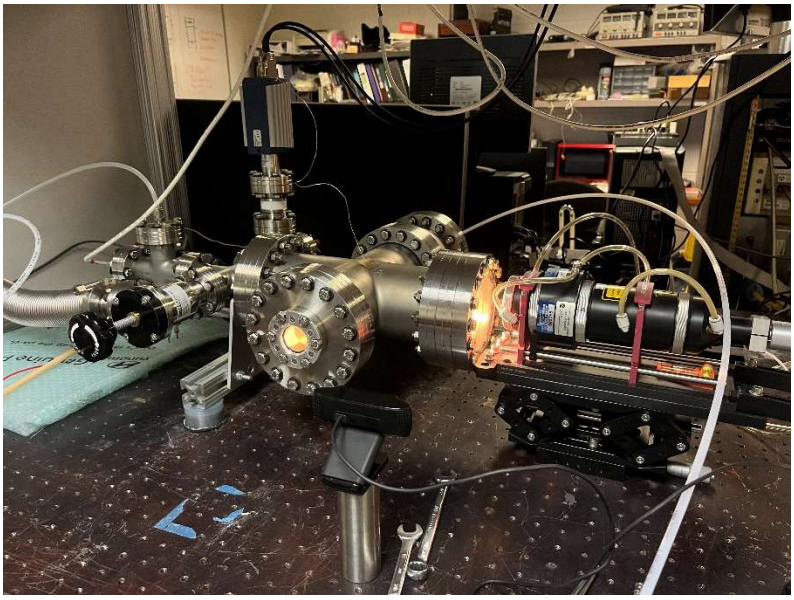

Fig. 2 Phase 2 Experimental Setup During Live Test

In the second phase of experiments, a larger vacuum chamber was used with a fused silica window, an integrated C-type thermocouple, a cold trap, and a pressure sensor (INFICON), as seen in Figure 2. Samples were placed in a reduced-pressure argon environment, below 1.0 × 10^ (-3) Torr, and exposed to similar laser conditions with an effective applied power density of approximately 470 W/cm². The thermocouple was initially placed on the back side of the carbon ablator plate to determine the temperature. The mounting mechanism was revised by securing the

thermocouple perpendicular to the incident beam, measuring the frontal surface temperatures. Samples were friction-held in place using Macor ceramic plates to insulate the material with a C-type thermocouple probe placed 1-3 mm outside the 11 mm × 11 mm laser square, seen in Figure 3b. During testing, this design configuration of ceramic was used in order to achieve maximum thermal isolation and therefore the highest temperatures possible. Moving the thermocouple to the lower front of the ablator increased the accuracy of the recorded temperatures, and it allowed a larger ceramic piece to be fixed to the back plate, raising the final temperatures, until repeated thermal shock caused a fracture to form. Six PICA samples were ablated with this setup under maximum laser power (12 V) and increasing time durations. Pre-and-post weight samples were taken to quantify the material ablation. After testing, X-ray micro-computed tomography (Zeiss Xradia Context MicroCT) was used to analyze internal failures in the ablator, characterize its degradation, and provide insight into how TPS materials respond to sustained localized heating.

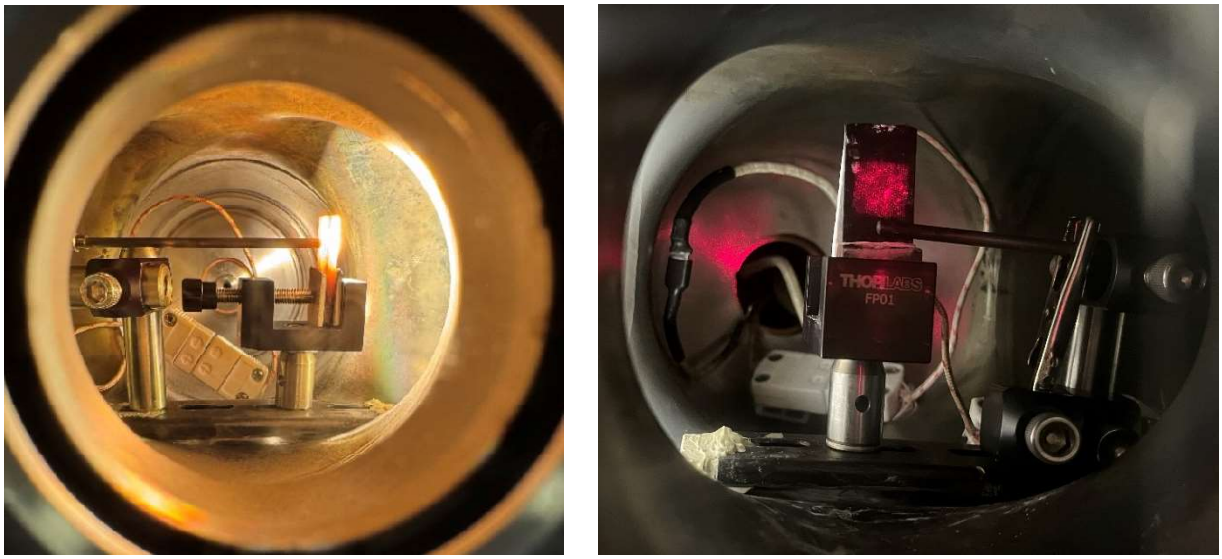

Fig. 3a (left) & 3b (right) Initial Test Setup vs Final with Variations of C-Type Thermocouple Placement

B. Laser Power and Heat Flux Calibration

During Phase 1, precise calibration of the laser and heat flux was essential to ensure accurate and reproducible results. The diode laser in this setup was reported to emit a continuous wavelength of 910 nm and achieve a theoretical peak power of 500 W. However, as shown in Figure 4, practical constraints limited the maximum recorded laser power to 450 W when inducing 4.32 V. Following this conclusion, a regression analysis of the data was performed. The data showed a strong linear correlation between the laser power and the input voltage, with an R^2 value of 0.9906. Similarly, calibration temperature measurements were conducted. A K-type thermocouple was placed on the surface of the PICA sample with its output linked to a data acquisition program to generate a temperature versus time graph, and a two-color pyrometer was secured outside the chamber. This setup allowed for precise monitoring of the sample's temperature response to laser heating through conduction and thermal radiation emission.

Voltage (V)	Power (W)
0.00E+00	0.00E+00
7.04E-01	2.13E+01
8.00E-01	3.94E+01
9.60E-01	6.03E+01
1.10E+00	8.38E+01
1.28E+00	1.02E+02
1.34E+00	1.18E+02
1.52E+00	1.40E+02
1.66E+00	1.60E+02
1.80E+00	1.79E+02
1.92E+00	1.98E+02
2.12E+00	2.20E+02
2.28E+00	2.40E+02
2.44E+00	2.62E+02
2.64E+00	2.80E+02
2.88E+00	3.03E+02
3.04E+00	3.20E+02
3.24E+00	3.41E+02
3.40E+00	3.59E+02
3.44E+00	3.82E+02
3.56E+00	4.01E+02
3.84E+00	4.18E+02
4.00E+00	4.37E+02
4.32E+00	4.49E+02

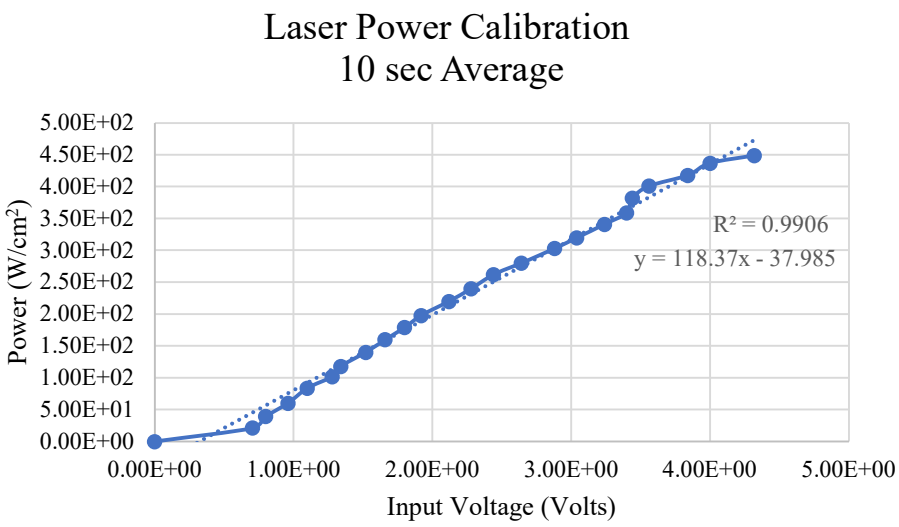

Fig. 4 Laser Power Output Versus Input Voltage, Showing Close Linear Fit

IV. Experimental Results

The results of Phase 1 demonstrated that measurable off-gassing was initiated by thermal loading from a high-powered laser. As the PICA material absorbed laser energy, it triggered thermal decomposition and combustion processes. To examine the material's response across a range of laser voltages, the experiment was conducted eight times under controlled conditions. For qualitative analysis of the gases released during pyrolysis, an HPR-20 mass spectrometer (MS) was used to extract samples from the gas flow before they condensed in the liquid nitrogen trap. Multiple gas species were detected at varying voltage levels; however, only the eight species seen in Figure 5 exhibited a significant and consistent presence.

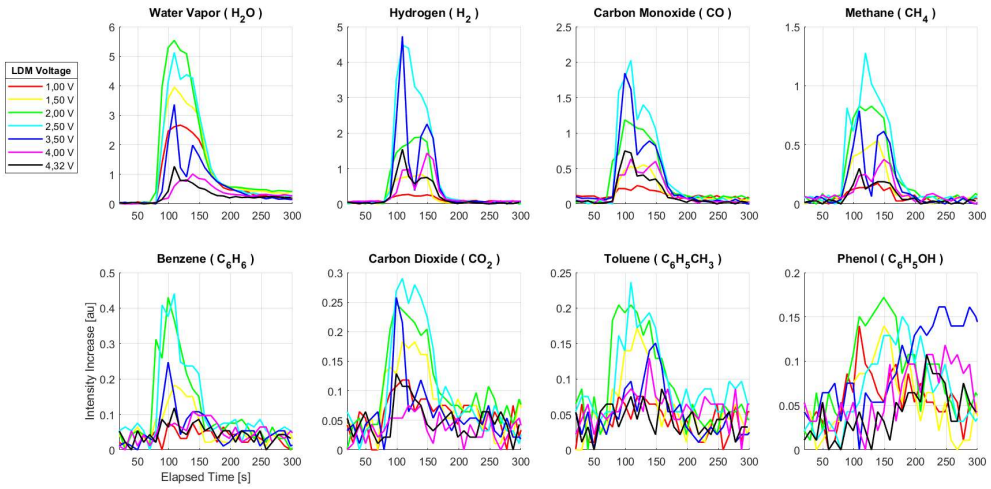

Fig. 5 Mass Spectrometer Gas Species Measurements versus Time

The gas analysis revealed that the majority of off-gassed species consisted of water vapor and hydrogen, with smaller but detectable quantities of methane and carbon monoxide. Notably, at voltages of 2.5 V and above, a distinct "dip" in gas output was observed. This is most prominent in the hydrogen signal at 3.5 V, suggesting that the laser may have penetrated completely through the sample at that point, abruptly altering the outgassing behavior.

As the laser voltage varied from 1 V to a maximum of 4.32 V, the sample temperature rose steadily, reaching 1350 °C before plateauing within a 23-second interval. This thermal behavior aligns with trends reported in *Performance of a Low-Density Ablative Heat Shield Material* [4]. As shown previously in Figure 4, every 0.5 V increment in voltage led to a proportional temperature increase of approximately 80-200 °C. At 2.5 V, tar-like residues were observed forming on the copper cylinder used to secure the sample, as well as visual degradation of the incident face, as visualized in Figure 6.

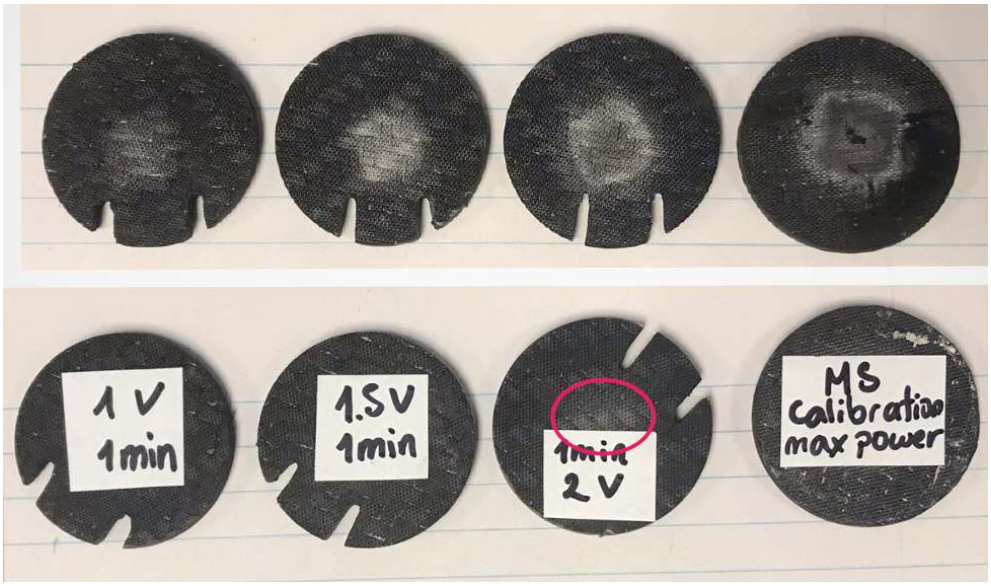

Fig. 6 Pica Samples with Varying Time Stamps and Voltage, Signs of Rear Degradation on the 1 Minute and 2 Volts Piece

The heat flux applied to the sample increased linearly with voltage, and this relationship is well-modeled by a linear function as depicted in Figure 4. With samples measuring 33.66 mm in diameter and 3.33 mm in thickness,

mass, volume, and thus material density were calculated accordingly. Using data from Figures 4 and 5, the material properties summarized in Figure 7 were derived. Despite being conducted in a helium atmosphere, the calculated properties showed comparable magnitudes to those observed in PICA materials ablated in air or methane environments using plasma wind tunnel testing. Interestingly, the 60-second laser ablation in helium achieved higher peak temperatures than 125-second ablations of PICA in air or CO_2 using a plasma torch, yet the percentage mass loss was similar. The impregnated carbon fiber sample with these conditions in Phase 1 exhibited a total mass loss of 16.38%.

Voltage (V)	Q (W)	ϕ ($W.m^{-2}$)	Energy (J)	Integrated Heat Input (J/m2)
1,00E+00	7,40E+01	6,12E+05	4,44E+03	3,67E+07
1,50E+00	1,35E+02	1,12E+06	8,10E+03	6,69E+07
2,00E+00	1,96E+02	1,62E+06	1,17E+04	9,71E+07
2,50E+00	2,57E+02	2,12E+06	1,54E+04	1,27E+08
3,00E+00	3,18E+02	2,62E+06	1,91E+04	1,57E+08
3,50E+00	3,78E+02	3,13E+06	2,27E+04	1,88E+08
4,00E+00	4,39E+02	3,63E+06	2,64E+04	2,18E+08
4,32E+00	4,78E+02	3,95E+06	2,87E+04	2,37E+08

maximum temperature (°C)	Thermal conductivity ($W.K^{-1}.mm^{-1}$)	Thermal Gradient ($K.mm^{-1}$)	heat of ablation ($J.Kg^{-1}$)
5,37E+02	-3,98E+03	1,54E+02	8,38E+06
6,85E+02	-5,63E+03	1,98E+02	1,53E+07
8,78E+02	-6,32E+03	2,56E+02	2,22E+07
9,55E+02	-7,60E+03	2,79E+02	2,91E+07
1,11E+03	-8,04E+03	3,26E+02	3,59E+07
1,32E+03	-8,05E+03	3,89E+02	4,28E+07
1,35E+03	-9,12E+03	3,98E+02	4,97E+07
1,35E+03	-9,93E+03	3,98E+02	5,41E+07

ablation time	60 s
surface (mm^2)	1,21E+02
volume (mm^3)	4,03E+02
density ($g.ml^{-1}$)	1,41E+00
initial temperature	25°C

Fig. 7 Material Properties and Test Results

The results of Phase 2 were dependent upon the six samples that were tested. Of the samples tested in Phase 2, the mass change varied from 0.20 g to 0.34 g with an average of 0.265 g, as seen in Figure 8. The mass difference increased with prolonged exposure time to the laser; however, exposure time greater than 3 minutes often yielded comparable mass drops. The material tested consisted exclusively of phenolic resin and carbon fiber. The phenolic resin, when exposed to thermal heating of 120 °C to 720 °C, decomposes and emits gases such as phenol, water vapor, methanol, and carbon dioxide [5]. Carbon fiber typically oxidizes and releases gases at 400 °C; however, when placed in an inert environment or a vacuum, carbon fiber may remain stable until 3000 °C, and it is resistant to chemical decomposition [6].

Piece #	Time (min.)	Volts	Temp (°C)	Initial Mass	Final Mass	Change in Mass
9	0.5	12	827	2.41	2.21	0.20
10	1.0	12	1075	2.37	2.16	0.21
11	2.0	12	1173	2.41	2.17	0.24
12	3.0	12	1085	2.33	2.04	0.29
13	4.0	12	1100	2.85	2.51	0.34
14	7.0	12	1130	2.81	2.50	0.31

Fig. 8 Results from Ablation of the Six Samples from Phase 2

The mass differences of the pieces in Phase 2 are strongly correlated with the gas analysis of Phase 1. Considering that carbon fiber is resistant to chemical decomposition within the temperature range of the experiment, the phenolic resin is likely the only component released by the samples. From Chung [6], the expectation of the gaseous emission from ablated phenolic resin consisted of significant amounts of water vapor, phenol, carbon monoxide, methane, and benzene emitted between temperatures of 580 °C to 720 °C, which is closely aligned with the results from the Phase 1 gas analysis. The significant gaseous emissions from Phase 1 tended to peak during a laser voltage of at least 2 V, which corresponded to a surface temperature of 878 °C, greatly exceeding the requirement for gas emission. The data from the gas analysis showed that detectable amounts of gases associated with the thermal decomposition of phenolic resin were present in the mass spectrometer species analysis of the ablated PICA. With significant evidence of phenolic resin undergoing thermal decomposition during the ablation process, it is likely that the decomposed phenolic resin

created the mass drop seen in the second stage of experimentation due to the chemical stability of carbon fiber and the tendency for phenolic resin to significantly thermally decompose over temperatures of 500 °C.

After testing concluded, CT was used on piece number 9 since the maximum recorded temperature reached 827 °C during a 30-second time interval. The non-ablated side shown in Figure 9 exhibits a uniform weave morphology with small, clustered darker void regions and limited structural degradation. In contrast, the ablated side, Figure 10, shows pronounced, larger cavities caused by localized pitting, evidence of phenolic resin breakdown. The carbon strands in sections have no discernible structural damage. These differences show substantial damage was caused by intense and prolonged thermal exposure, leading to extensive carbon-phenolic matrix decomposition.

To quantify the sliced plane surface damage, the grayscale intensity profiles were extracted from the reconstructed recon 3D tomographic image using FIJI. The attenuation rate of voids or air caused darker pixel values, providing a relative measure of roughness amplification caused by material degradation. The backside surface reveals a mean gray value of approximately 4800-5000 with a peak-to-valley variation of 500-700 gray levels, reflecting lower amplitude but higher frequency fluctuations consistent with intact carbon inter-weaved matrices. In contrast, the laser-heated surface exhibits a reduction in mean gray value, approximately 4400-4700, and a peak-to-valley variation exceeding 1500 gray levels. The grayscale variation increases by a factor of 2.5 relative to the back face, which confirms significant roughness amplification due to deep localized troughs caused by nonuniform material removal. Comparing the pixel widths between each trough amplitude allows for a relative comparison of trough size. The laser-ablated side has an average pixel gap width of 35 pixels, while the back face trough width is less than 10 pixels. The voids within the laser-heated side are larger and deeper in comparison.

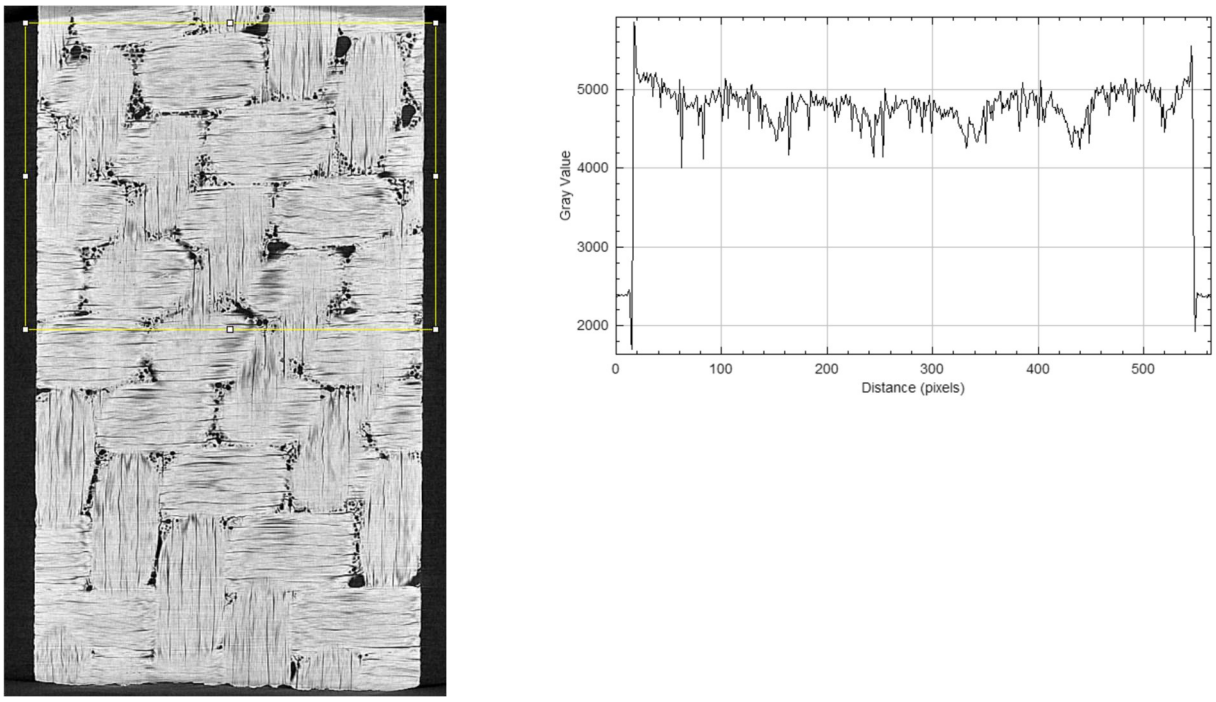

Fig. 9a & 9b PICA Rear Lower Internal Slice Revealing Smaller, Densely Packed Voids, and corresponding mean gray value graph

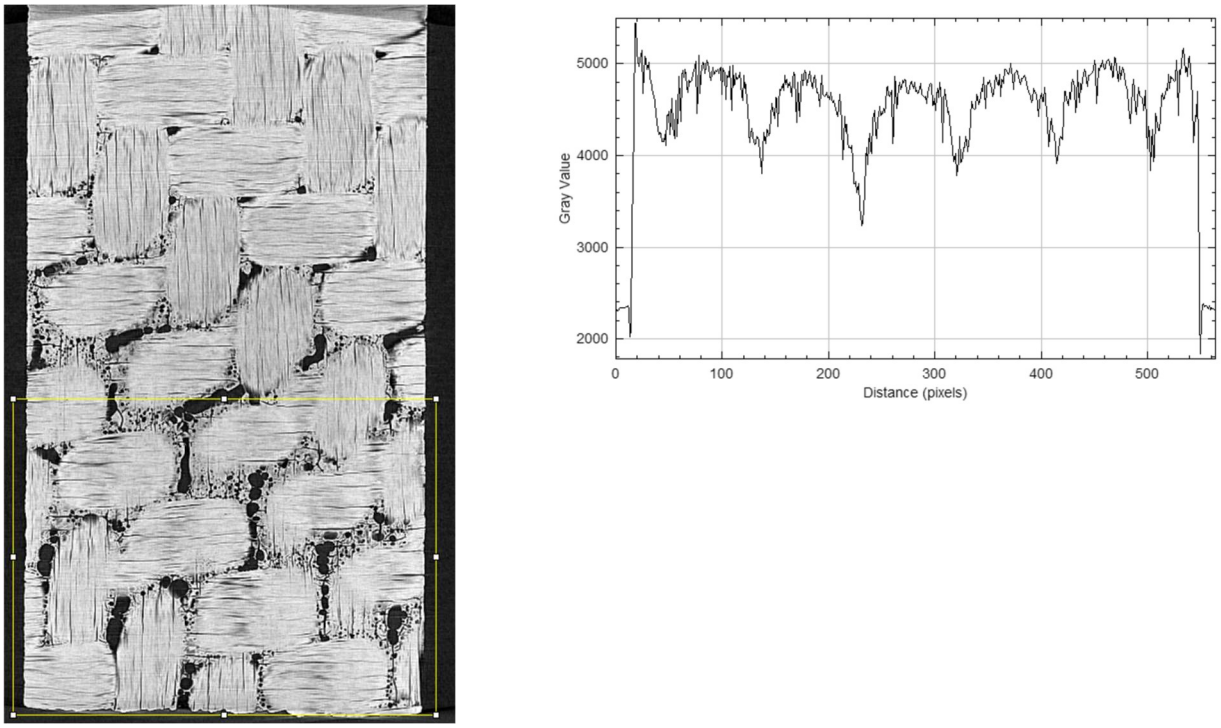

Fig. 10a & 10b PICA Front (Laser Incident) Top Internal Slice Revealing Larger, Conglomerated Voids, and corresponding mean gray value graph

The temporal evolution of the major outgassing species measured during testing, Figure 5, provides direct correlation with the observed morphological changes. Water vapor (H_2O) and Hydrogen (H_2) demonstrate strong peaks between approximately 80 and 130 seconds, with applied laser voltage until the laser penetrates through the sample, as discussed previously. Water vapor production is associated with dehydration and oxidation reactions within the phenolic matrix, and its early appearance indicates rapid thermal decomposition. Hydrogen generation, caused by resin pyrolysis and cracking reactions, contributes to internal gas pressurization that allows fiber-matrix debonding and micro-void expansion. Phenol (C_6H_5OH), a primary decomposition product of phenolic resin, shows the deterioration over a broader time interval, indicating continuous matrix mass loss within the heated region. This sustained resin depletion explains the increased void proportions and the periodic intensity troughs aligned with weave architecture.

V. Conclusion

This investigation provides a comprehensive experimental assessment of the thermo-chemical and microstructural response of PICA material under sustained, high-power laser heating. By combining the gas analysis results of the first phase of experimentation with the post-test X-ray tomography, this study relates the volatile emission and resin decomposition with the structural degradation of TPS materials.

And while this study provides an effective evaluation of PICA material under high-power laser heating, several limitations should be acknowledged. The chemical analysis of volatile emissions was constrained by access to a mass spectrometer beyond the work in Phase 1, disallowing multiphase evaluation of any particular sample. Minor inconsistencies regarding thermocouple placement in both setups also contributed to variability in recorded surface temperatures, which is significant given the inherent steep thermal gradients present in ablative materials under thermal loading. Post-test analysis using the Zeiss Xradia Context MicroCT was also limited by the similar X-ray attenuation coefficients of carbon fiber and the residual phenolic, complicating the material analysis of the ablated samples.

Phase 1 testing confirmed substantial outgassing of various compounds, including phenol, which, supported by the residue left in Phase 2 testing, suggests active phenolic pyrolysis under thermal loading. Phase 2 experiments, conducted in a reduced-pressure argon environment, demonstrated consistent mass loss and offered insight into the temperature-specific breakdown of PICA materials. Post-test CT analysis identified measurable degradation within

samples, confirming that resin decomposition is not limited to the surface, but rather that it impacts the material structure deep within the composite.

The mass loss in Phase 2 experimentation was consistent with an average of 0.265 g, and it substantiates the conclusion that the increase in void presence at the ablation site is a direct result of the off-gassing found in Phase 1. Further, in combination with the x-ray analysis, this suggests that heat effects penetrate the surface of the ablator material and simultaneously degrade the entire structure at varying depths consistently.

This work demonstrates that sustained thermal loading induces significant physical and chemical changes in PICA material, and it characterizes the isolated thermal impacts of high enthalpy aerospace applications. Future work should incorporate microstructural and volatile emission analysis on common samples to better correlate chemical and structural impacts, nonintrusive thermal diagnostics to eliminate precision errors, and multi-modal characterization techniques to better differentiate material phases in post-test analysis. Extending this experimental framework to additional impregnated carbon and phenolic-based ablative TPS materials will enable direct comparison of structural degradation and help determine whether the recorded data are characteristic of similar systems, thereby supporting more predictive modeling and material selection for extreme heat-flux aerospace environments.

Appendix

Acknowledgments

This work is supported by the United States Navy Joint Hypersonics Transition Office. Thank you to the University of Tennessee's Advanced Microscopy and Imaging Center and Stephen Young for support with CT software.

VI. References

[1] S. Sepka, M. Gasch, R. A. Back and S. White, "Testing of Candidate Rigid Heat Shield Materials at LHMEL for the Entry, Descent, and Landing Technology Development Project," *Proc. 36th Int. Conf. on Advanced Ceramics and Composites*, Daytona Beach, FL, 2012.

[2] K. Daryabeigi and E. Kurz, "Transient Radiant Thermal Testing of Reusable Thermal Protection Systems and Insulation Materials," NASA Technical Memorandum TM-20250004276, NASA Langley Research Center, Hampton, VA,, 2025.

[3] A. Bryan and et, Al., "Multiscale Structural Evolution and Permeability in a Commercial Carbon/Carbon Composite under Arc-Jet Ablation," *Carbon Trends,* vol. vol. 22, p. p. 100604, 2026.

[4] M. A. Covington, J. M. Heinemann, H. E. Goldstein, Y. -K. Chen, I. Terrazas-Salinas, J. A. Balboni, J. Olejniczak and E. R. Martinez, ""'Erratum on 'Performance of a Low Density Ablative Heat Shield Material'"," *Journal of Spacecraft and Rockets,* vol. 2, no. 45, pp. 237-247, July 2008.

[5] A. Bobrowski, D. Drożyński, B. Grabowska, K. Kaczmarska, Z. Kurleto-Kozioł, M. Brzeziński, "Studies on thermal decomposition of phenol binder using TG/DTG/DTA and FTIR-DRIFTS techniques in temperature range 20-500 °C," *China Foundry,* Vol. 15, No. 2, 2018, pp. 145-151

[6] D. Chung, "Properties of Carbon Fibers," *Carbon Fiber Composites,* Butterworth-Heinemann, 1994, pp. 65-78